# Antimicrobial Peptides Temporins B and L Induce Formation of Tubular Lipid Protrusions from Supported Phospholipid Bilayers

Yegor A. Domanov and Paavo K. J. Kinnunen
Helsinki Biophysics & Biomembrane Group, Medical Biochemistry/Institute of Biomedicine, University of Helsinki, Helsinki, Finland

ABSTRACT The binding of the antimicrobial peptides temporins B and L to supported lipid bilayer (SLB) model membranes composed of phosphatidylcholine and phosphatidylglycerol (4:1, mol/mol) caused the formation of fibrillar protrusions, visible by fluorescent microscopy of both a fluorescent lipid analog and a labeled peptide. Multicolor imaging at low peptide-to-lipid ratios ($P/L < \sim 1{:}5$) revealed an initial in-plane segregation of membrane-bound peptide and partial exclusion of lipid from the peptide-enriched areas. Subsequently, at higher P/L numerous flexible lipid fibrils were seen growing from the areas enriched in lipid. The fibrils have diameters <250 nm and lengths of up to ~1 mm. Fibril formation reduces the in-plane heterogeneity and results in a relatively even redistribution of bound peptide over the planar bilayer and the fibrils. Physical properties of the lipid fibrils suggest that they have a tubular structure. Our data demonstrate that the peptide-lipid interactions alone can provide a driving force for the spontaneous membrane shape transformations leading to tubule outgrowth and elongation. Further experiments revealed the importance of positive curvature strain in the tubulation process as well as the sufficient positive charge on the peptide ($\geq +2$). The observed membrane transformations could provide a simplified in vitro model for morphogenesis of intracellular tubular structures and intercellular connections.

## INTRODUCTION

Synthesis and secretion of antimicrobial peptides (AMPs) constitute an important element of innate immunity in all organisms ranging from prokaryotes to humans. In higher animals, AMPs provide the first line of defense against microbial infection because of their ability to quickly kill various pathogens in locations, such as skin, mucosae, and lesions, exposed to the external environment (1,2). AMPs isolated from different sources exhibit varying degrees of specificity for bacteria, fungi, and enveloped viruses, often combined with a low toxicity to eukaryotic cells (3). The above characteristics of AMPs have inspired intensive research into their mechanisms of action and selectivity, aiming at the development of a new family of antibiotics less amenable to the development of bacterial resistance (3).

It is now widely accepted that central to the bactericidal activity of most AMPs is their interaction with bacterial membrane(s). More specifically, their toxicity appears to be related to the disruption of the surrounding lipid bilayer or effects on certain cytoplasmic targets after peptide translocation through the membrane. Accordingly, irrespective of the tissue and organisms from which they are isolated, all AMPs share common physicochemical features, which facilitate their accumulation on and interaction with bacterial membranes. In brief, these molecules possess a net positive charge, with the lower limit of +2, and in their active conformation hydrophilic and hydrophobic residues are segregated, yielding a highly amphiphilic overall structure (4,5). On the other hand, their selectivity against particular microbial pathogens appears to be related to rather subtle variations in both peptide structure (charge, conformation, amphipathicity, hydrophobicity) and membrane lipid composition (charge density, unsaturation, curvature strain, presence of sterols). Numerous studies have been devoted to the determination of minimal structure and sequence requirements for AMP activity and selectivity (6,7).

The current investigation is focused on the antimicrobial peptides from the temporin family, first isolated from the skin secretion of European red frog *Rana temporaria* (8). These peptides are of particular interest because they contain only 10 to 13 residues and thus are among the shortest AMPs found to date. Moreover, unlike other known short AMPs (e.g., indolicidin, 13 amino acids, and bactenecin-1, 12 amino acids), temporins are weakly charged linear peptides composed of conventional amino acids. Despite their small size and weak charge, temporins cause significant perturbations

*Submitted June 20, 2006, and accepted for publication September 1, 2006.*

Address reprint requests to Paavo K. J. Kinnunen, Helsinki Biophysics & Biomembrane Group, Medical Biochemistry/Institute of Biomedicine, PO Box 63 (Haartmaninkatu 8), FIN-00014 University of Helsinki, Finland. Tel.: 358-9-19125400; Fax: 358-9-19125444; E-mail: paavo.kinnunen@helsinki.fi.

*Abbreviations used*: SLB, supported lipid bilayer; AMP, antimicrobial peptide; MIC, minimal inhibitory concentration; CL, cardiolipin; PC, phosphatidylcholine; PG, phosphatidylglycerol; SOPC, 1-stearoyl-2-oleoyl-*sn*-glycero-3-phosphocholine; POPG, 1-palmitoyl-2-oleoyl-*sn*-glycero-3-phospho-*rac*-glycerol; POPE, 1-palmitoyl-2-oleoyl-*sn*-glycero-3-phosphoethanolamine; NBD-PC, 1-oleoyl-2-[12-[(7-nitro-2-1,3-benzoxadiazol-4-yl) amino]dodecanoyl]-*sn*-glycero-3-phosphocholine; NBD-PG, 1-oleoyl-2-[12-[(7-nitro-2-1,3-benzoxadiazol-4-yl)amino]dodecanoyl]-*sn*-glycero-3-[phospho-*rac*-(1-glycerol)]; HPLC, high performance liquid chromatography; TR, Texas red (Sulforhodamine 101); temB, temporin B (LLPIVGNLLKSLL-$NH_2$); C-temB-COOH, temporin B variant with a cysteine added at the N-terminus and a carboxylic function at the C-terminus (CLLPIVGNLLKSLL-COOH); C-temB-K, temporin B variant with a cysteine added at the N-terminus and L→K substitution at the C-terminus (CLLPIVGNLLKSLK-$NH_2$); temL, temporin L (FVQWFSKFLGRIL-NH2). P/L, peptide-to-lipid molar ratio; wt, wild type.



0006-3495/06/12/4427/13 $2.00 doi: 10.1529/biophysj.106.091702

of membrane structure (9–11). Temporins A and B are active against gram-positive bacteria minimal inhibitory concentration (MIC) in the range of 2–5 $\mu$M), protozoa (*Leishmania donovani*), and fungi (*C. albicans*) but show no hemolytic activity (8,12). Temporin L was found to be less selective, efficiently killing both gram-positive and -negative bacteria, fungi, and cancer cells and lysing erythrocytes (11). Studies on the mechanisms of antimicrobial effect of temporins have revealed that their activity is mediated by disruption of the plasma membrane rather than by a receptor-mediated pathway or by affecting some specific target inside the cell (11,13). Similarly to some other AMPs, temporins act synergistically with the antimicrobial secretory phospholipase $A_2$, enhancing its activity (14). Temporins thus represent a good minimal model for membrane-destabilizing peptides with varying selectivity. In addition, their antimicrobial activity was shown to be relatively insensitive to ionic strength (12), which together with their selective activity against different types of cells makes these peptides promising for possible pharmacological applications.

A wide variety of model membrane systems and membrane mimetic environments have been employed in biophysical studies on the interactions of AMPs with membranes, including Langmuir monolayers, large unilamellar vesicles, giant liposomes, and micelles (10,15,16). However, use of supported lipid bilayers (SLBs) has so far been more limited. Yet, because of the well-defined bilayer geometry and confinement on a solid support, this membrane model is of particular interest when combined with surface-sensitive microscopic and spectroscopic techniques. Here we describe morphological transformations of a glass-supported phospholipid bilayer in response to binding of temporin B (wild type and two variants), temporin L, and melittin observed using fluorescence microscopy. In brief, these amphiphilic peptides were found to initiate a rapid outgrowth of flexible fibrils from the surface of the supported bilayer. The fibrils were composed of both lipid and the amphiphilic peptide. Characteristics of these fibrils further indicated them to have a tubular structure. Wild-type temporin B was found to be the most effective, giving rise to numerous long (up to several hundred micrometers) tubules. The extent and morphological features of peptide-induced perturbations were found to be very sensitive to modifications of the peptide sequence as well as to the SLB lipid composition, with lipids having negative spontaneous curvature attenuating the tubulation.

## EXPERIMENTAL PROCEDURES

### Materials

Hepes, EDTA, bovine heart cardiolipin (CL), hen egg lysozyme, and horse heart cytochrome *c* were from Sigma (St. Louis, MO). 1-Stearoyl-2-oleoyl-*sn*-glycero-3-phosphocholine (SOPC), 1-palmitoyl-2-oleoyl-*sn*-glycero-3-phospho-*rac*-glycerol (POPG), 1-palmitoyl-2-oleoyl-*sn*-glycero-3-phosphoethanolamine (POPE), 1-oleoyl-2-[12-[(7-nitro-2-1,3-benzoxadiazol-4-yl) amino]dodecanoyl]-*sn*-glycero-3-phosphocholine (NBD-PC), 1-oleoyl-2-[12-[(7-nitro-2-1,3-benzoxadiazol-4-yl)amino]dodecanoyl]-*sn*-glycero-3-[phospho-*rac*-(1-glycerol)] (NBD-PG) were from Avanti Polar Lipids (Alabaster, AL). Texas red $C_2$-maleimide was from Molecular Probes (Eugene, OR).

Temporins and their variants were from SynPep (Dublin, CA). Their purity was checked by HPLC (>95%) and compositions confirmed by mass spectrometry. Sequences and structural details of these peptides are compiled in Fig. 1. Bee venom melittin from Sigma was used after additional purification by HPLC (purity > 95%).

Unless otherwise indicated, all experiments were carried out in buffer containing 20 mM Hepes, 0.1 mM EDTA, pH 7.0, and prepared using Milli-Q water.

### Fluorescence labeling of the peptides

To avoid aggregation and precipitation of Texas Red maleimide and/or the peptide during conjugation, the labeling was done in mixed organic/aqueous buffer solution: 20% acetonitrile in 20 mM Hepes, 0.1 mM EDTA, pH 7.0. Texas red maleimide and cysteine-containing variants of temporin B were mixed in 1:1 molar ratio at final concentrations of 50 $\mu$M. The mixture was incubated for 3 h in the dark with stirring. Labeled peptide was purified by reversed-phase HPLC ($\mu$RPC C2/C18 ST 4.6/100 column, ÄKTÄ Purifier 10 system, Amersham Biosciences, Uppsala, Sweden) and eluted with a linear gradient from 20% to 80% acetonitrile with 0.05% trifluoroacetic acid. No unreacted Texas red maleimide was detected, indicating that the peptide was completely labeled. This was further confirmed by mass spectrometry using a flexControl MALDI-TOF spectrometer (Bruker Daltonics, Bremen, Germany) and a saturated solution of $\alpha$-cyano-4-hydroxycinnamic acid as a matrix.

### Preparation of supported bilayers

Standard glass coverslips (22 × 22 mm, O. Kindler, Freiburg, Germany) and Lab-Tek chambered coverglasses (Nunc A/S, Roskilde, Denmark) were

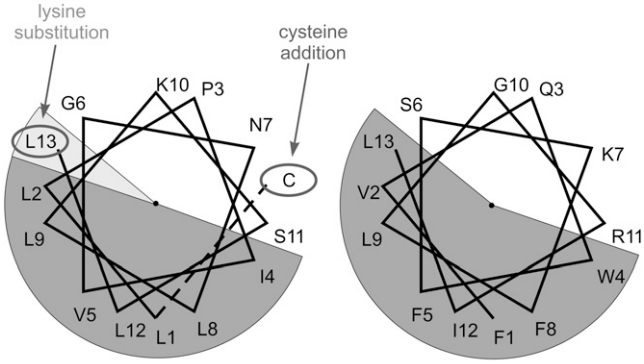


FIGURE 1 Sequences and helical wheel diagrams of temporins used in the study. Segregated hydrophobic residues in $\alpha$-helical conformation are highlighted by gray shading. Radii of the unshaded sector subtend the peptide's polar angle. Sites of modifications in the temporin B variants are shown within ovals. C-temB-COOH variant contains cysteine addition at the N-terminus and a carboxylic group at the C-terminus, C-temB-K variant has cysteine addition at the N-terminus and L→K substitution at the C-terminus.

cleaned by sonication for 30 min in 2% Hellmanex II cleaning solution (Hellma, Müllheim, Germany) at ~50°C. The coverglasses were used within 12 h after cleaning and were thoroughly rinsed with hot tap water, ethanol, and Milli-Q water immediately before use.

Lipid vesicles were prepared as follows. Appropriate amounts of lipid stock solutions were mixed in chloroform to obtain the desired compositions, with fluorescent lipid derivatives NBD-PC or NBD-PG constituting 2 mol % of total lipid. The solvent was removed under a stream of nitrogen, and the lipid residue was subsequently maintained under reduced pressure for at least 1 h. The dry lipids were hydrated with buffer at room temperature. The resulting dispersions were extruded through a polycarbonate filter (50-nm pore size, Millipore, Bedford, MA) using a LiposoFast low-pressure homogenizer (Avestin, Ottawa, ON) to obtain unilamellar vesicles.

SLBs were formed by vesicle fusion (17,18). To avoid exposure of supported membrane to air, bilayers were formed directly in microscopy observation chambers. Both commercial chambered coverglasses (Lab-Tek) and homemade chambers, consisting of a glass frame to which two coverslips are attached using silicon grease, were used for microscopy. Chambers were filled with liposome suspension containing 100 $\mu$M total lipid and 5 mM $CaCl_2$, the latter added immediately before the bilayer deposition. After incubation for 20 min in the dark, excess liposomes were washed with at least 20 ml of buffer run through the chamber, and the final volume of solution in each chamber was adjusted to 600 $\mu$l.

In most of the experiments, we used membranes composed of SOPC and POPG in molar ratio of 8:2. Twenty percent of PG imparts a sufficient negative surface charge to the bilayer, thus ensuring efficient association of the cationic peptides, as occurs on bacterial membranes. On the other hand, this percentage of the acidic lipid is not too high to hamper reproducible vesicle fusion and SLB formation (18).

The supported bilayers were examined visually by epifluorescence (19). After washing, SLBs revealed uniform surface fluorescence without dark defects or bright spots caused by adhering lipid particles. Continuity of the SLBs was confirmed by fluorescence recovery after photobleaching, with the dark bleached spot, observed after intense excitation light illumination, dissipating in ~20–30 min for a continuous bilayer in which lateral diffusion of the fluorescent lipid molecules is not obstructed.

Total amount of lipid in an SLB was determined by solubilizing SLBs with 1% Triton X-100. Fluorescence spectra of solubilized lipids were then recorded (Cary Eclipse, Varian, Mulgrave, Victoria, Australia) with excitation at 470 nm and bandpasses of 20 and 5 nm for excitation and emission, respectively. Integrated intensity under these spectra was compared to that of the reference sample of solubilized fluorescent liposomes with known amount of lipid. Glass surface was found to accommodate 525 $\pm$ 8 pmol of lipid per 1 $cm^2$, which corresponds to mean area per lipid of 0.63 $nm^2$, in good agreement with the values estimated for phospholipid bilayers (20).

## Fluorescence microscopy

Epifluorescence from supported membranes was observed with an inverted microscope (IM-35, Zeiss, Jena, Germany) using a 40× Neofluar objective and a mercury arc lamp as an excitation source. Filter sets appropriate for the observation of NBD (BP450-490, FT510, LP520) and Texas Red (BP546/12, FT580, LP590) were used. A neutral-density filter (optical density 1.0) was used to attenuate the excitation light.

Confocal fluorescence microscopy was performed using an inverted microscope (IX 70, Olympus, Tokyo, Japan) equipped with a spinning disk confocal scanner (CSU10, Yokogawa, Tokyo, Japan) and a krypton argon ion laser (Melles Griot, Carlsbad, CA). The argon line at 488 nm was used for NBD excitation, and a long-pass filter for emission. High-resolution imaging was carried out with an oil immersion 100× objective (UPlanSApo, Olympus).

Fluorescence images were collected using a Peltier-cooled 12-bit B/W CCD camera (C4742-95, Hamamatsu, Hamamatsu City, Japan) interfaced to a computer and operated by the software (HiPic 5.1 or AquaCosmos 1.2) provided by the camera manufacturer. Additional image processing was done using ImageJ software developed at NIH/RSB (21).

## Microinjection

Micropipettes with inner tip diameter of ~10 $\mu$m were made from borosilicate capillaries (1.0 mm o.d., 0.58 mm i.d.) by a microprocessor-controlled horizontal puller (P-87, Sutter Instrument, Novato, CA). Micropipettes were positioned several micrometers over the supported bilayer using motorized micromanipulators (MX831/MC2000, SD Instruments, Grants Pass, OR). Temporin B solution (20 $\mu$M in 20 mM Hepes, 0.1 mM EDTA, pH 7.0) was injected pneumatically as a continuous flow with a flow rate of ~100 nl/s using a syringe actuated by a micrometer screw.

# RESULTS

## Tubule formation

Interactions between the indicated amphiphilic peptides and SLBs were studied by adding the former either into the bulk of the solution contacting the bilayer or by local application over a small area of the membrane. In the first set of experiments, we used the antimicrobial peptide wt-temB, which was added into the buffer in the observation chamber (final concentration 0.1–2.5 $\mu$M) and the contents mixed by gentle repeated suction and dispensing using a handheld pipette. Accordingly, the bulk peptide concentration and hence the total peptide/lipid ratio (P/L) is defined. Because the membrane association of temB is enhanced by acidic phospholipids, SLBs composed of phosphatidylcholine (PC) and phosphatidylglycerol (PG) in molar ratio of 8:2 were employed. Before the addition of the antimicrobial peptide, the SLBs were characterized by a uniform NBD fluorescence (Fig. 2 *A*), with occasional bright dots most likely representing bilayer imperfections. Interestingly, the addition of temporin B triggers a rapid (<30 s) outgrowth of long fluorescent fibrils (Fig. 2 *B*), which are influenced by the liquid flow and undergo rapid Brownian motion (see complementary material), revealing high flexibility and evidently a small diameter. The length of the fibrils varies from <1 $\mu$m to hundreds of micrometers, depending on the peptide concentration (see below). The persistence length of the fibers is estimated to be on the scale of 1–5 $\mu$m. The transverse dimensions of these structures are beyond the resolution of optical microscopy (i.e., below ~250 nm). The even fluorescence evident along the whole length of fibrils suggests that their thickness is uniform along the fibril and is similar in different fibrils when the SLB is exposed to the same peptide concentration. The fibrillar structures normally extend out of the supported bilayer with one end fixed at the surface, being immobile and remaining in focus exactly at the surface. Instead, the loose end is moving freely in the aqueous phase and is observed in focus several micrometers from the surface. Occasionally the fibrils detach from the SLB and float freely close to the surface with both ends loose. The formation of the fibrils does not lead to the development of any apparent defects in the bilayer. The fibrils seem to grow more readily from the edges of preexisting bilayer defects or at the bilayer boundaries (Fig. 2 *C*). These fibrillar structures were not seen in control experiments in which plain buffer was added.

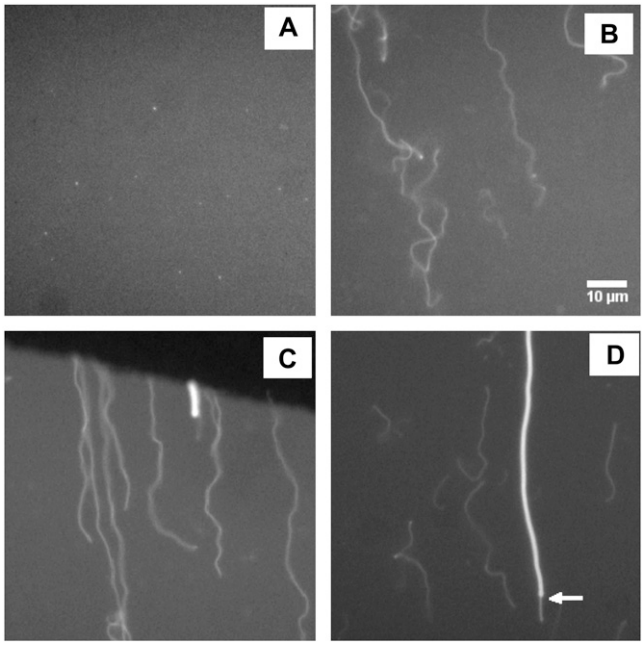


FIGURE 2 Temporin B induced formation of fibrillar lipid structures from a supported bilayer. The fluorescence images were taken before (*A*) and after (*B–D*) the addition of temB to yield a final peptide concentration of 0.3 $\mu$M ($P/L = 1{:}7.8$). Lipid composition of the bilayer was SOPC/POPG/NBD-PC, 78:20:2 (mol/mol). Some parts of the fluorescent threads are seen to be out of focus, revealing that they protrude out of the SLB plane. Differences in the intensity of the background surface fluorescence (*B–D*) are mainly to the result of rapid photobleaching of NBD. The boundary between the supported bilayer and bare glass is visible in *C*.

The fibrils appear to be quite stable, maintaining their length and shape on the time scale of tens of minutes. However, some of them undergo abrupt morphological changes with time. More specifically, a long thin fibril occasionally collapses into a shorter and thicker structure, which is less susceptible to fast Brownian motion, indicating increased rigidity. Such a thicker structure is depicted in Fig. 2 *D*, together with the remaining thinner filament from which it originated (*white arrow*). Judging by the high fluorescence from the interior of the thicker fibril, it has a multilamellar structure, because for a hollow unilamellar structure we would observe more fluorescence from the periphery than from the center. These cylindrical structures occasionally collapse further into spherical multilamellar liposomes. Although these morphological transformations are quite rare (e.g., one out of 10–50 thin fibers collapsed in 1 min), they were consistently seen in different samples.

The fibrils could be stretched by pulling their free end with a micropipette and were found to withstand more than a twofold increase in length, with a significant decrease of their apparent thickness upon stretching. These findings are consistent with the notion of a tubular as opposed to the cylindrical-micellar structure of the lipid protrusions (see Discussion). Thus, based on the features mentioned above, we may conclude that the fibrillar structures are tubules formed by a closed lipid bilayer with diameters below the light diffraction limit, i.e., below ~250 nm.

To follow the dynamics of tubule formation in response to a local increase in peptide concentration, temporin B was added onto a small area of SLB. Shown in Fig. 3, *A–D*, is a time-lapse sequence of images made during the peptide addition over PC/PG/NBD-PC (78:20:2, mol/mol) bilayer (pipette tip is located in the lower right-hand corner). Tubule formation starts immediately on the contact of peptide with the SLB, and the fluorescence from the membrane exposed to the peptide becomes attenuated. The area of decreased fluorescence expands progressively during the application and is accompanied by an increase in the number of tubules. Some of these structures remain attached to the surface, and others detach and move beyond the periphery of the site of application. To study if the acidic phospholipid from the PC/PG bilayer becomes incorporated into the tubular structures, NBD-PG was used instead of NBD-PC (see Fig. 7 *D*). In this case, fluorescence from both the SLB and the lipid tubules was observed, which confirms that the charged lipid component redistributes between the planar bilayer and the tubules without marked preference for a type of membrane organization. Similarly to the experiments with the peptide added to the bulk solution, application of buffer alone did not perturb the bilayer.

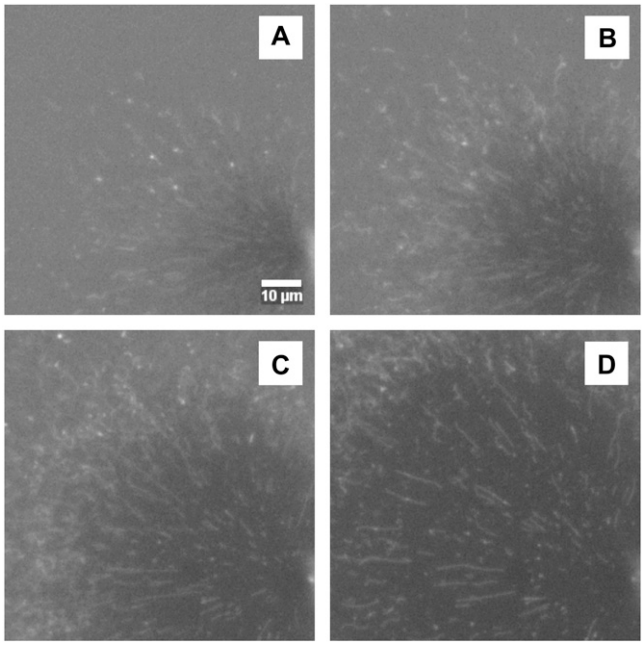


FIGURE 3 Localized addition of peptide by microinjection. Time-lapse sequence of images acquired 1, 2, 5, and 10 s (*A–D*, respectively) after the beginning of peptide injection over the bilayer composed of SOPC/POPG/NBD-PC, 78:20:2 (mol/mol). Temporin B solution (20 $\mu$M) was injected continuously with a flow rate of ~100 nl/s. Micropipette tip is located in the lower right corner of the images.

## Comparison of different peptides

To ascertain if the tubule formation described above is specific to temporin B, we investigated other membrane-active peptides and proteins. Temporin B variants used were C-temB-COOH and C-temB-K, which both have an additional cysteine residue at the N-terminus to allow labeling with thiol-reactive fluorescent probes. The former variant has a carboxyl group at the C-terminus, whereas the wild-type peptide and C-temB-K are amidated. In the latter peptide, the C-terminal leucine is further substituted for lysine to increase the polar angle (see Fig. 1). We also studied temporin L, another antimicrobial peptide of the temporin family, which differs from temporin B in its membrane association and target cell specificity (10). Melittin was selected because its interactions with membranes have been extensively studied (22–24). Finally, two water-soluble basic proteins associating with acidic phospholipids, cytochrome *c* and lysozyme, were also investigated.

Both wild-type temB and its C-temB-K variant induced rapid formation of tubules (Fig. 4, *A* and *C*, respectively). In contrast, even relatively high concentrations of C-temB-COOH (up to $P/L = 1:1$) did not induce tubules. At $P/L = 1:1.4$, heterogeneous surface fluorescence was observed (Fig. 4 *B*), whereas at $P/L = 1:7$ no membrane perturbation was evident at all (data not shown). TemL produced lipid structures of varying morphology including thin tubules similar to those formed by temB, thicker tubules, and multilamellar vesicles of different size (Fig. 4 *D*). Addition of relatively low quantities (0.33 $\mu$M or $P/L = 1:7$) of melittin gave rise to the formation of numerous relatively short tubules (Fig. 4 *E*), many of which featured stable regions of different thickness (*inset*). In contrast to the above amphiphilic peptides, cytochrome *c* and lysozyme caused very different changes in the organization of SLB, and their addition caused large areas with increased surface fluorescence. These areas are not vesicular structures and in general remain in the plane of the SLB, being in focus at the level of the SLB and characterized by a stepwise change in fluorescence intensity (Fig. 4 *F*, *inset*). Interestingly, the step size between the areas of different intensity is discrete and approximately equals the intensity level of the parent bilayer (quantified after subtraction of camera noise). Significantly lower overall fluorescence was observed for cytochrome *c*, which is readily explained by efficient resonance energy transfer from NBD to the heme moiety of this protein.

The above experiments also revealed tubule formation to depend on the peptide concentration. After the addition of 0.5 $\mu$M ($P/L = 1:4.7$) of temporin B variant C-temB-K (Fig. 1), initially uniform surface fluorescence (Fig. 5 *A*) became heterogeneous (Fig. 5 *B*). Because of the resolution limit of the optical system used, it was not possible to determine exactly what structures account for this heterogeneity. However, it can be surmised that the spots with higher fluorescence intensity are bundles of very short nanotubules or areas with increased surface density of lipid (compared to the darker areas). Confocal microscopy at higher magnification revealed that the bright areas (Fig. 5 *B*) consist of clusters of smaller, intensely fluorescent microdomains (Fig. 5 *E*). Further addition of the peptide (up to $P/L = 1:2.8$, Fig. 5 *C*) caused short lipid tubules to appear, while at the same time the background fluorescence from the supported bilayer became

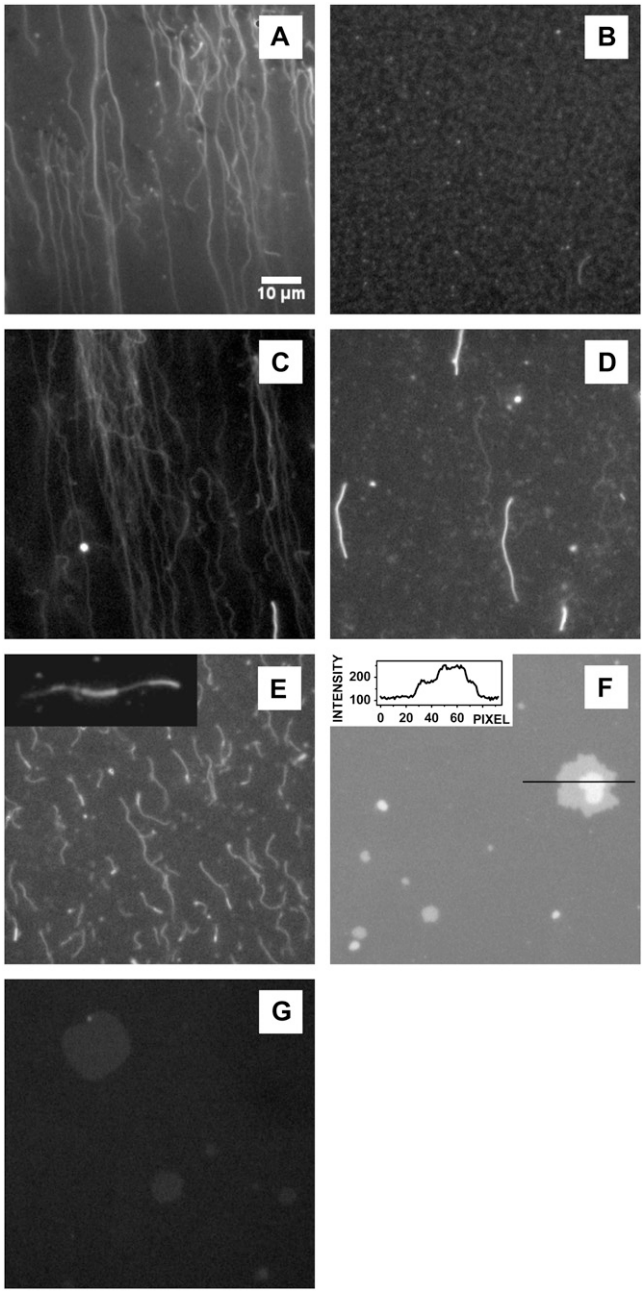


FIGURE 4 Effect of different membrane-active peptides and proteins on supported bilayers. The bilayers were imaged after bulk addition of wt-temB at $P/L = 1:7.8$ (*A*), C-temB-COOH at $P/L = 1:1.4$ (*B*), C-temB-K at $P/L = 1:1.4$ (*C*), tpL at $P/L = 1:2.8$ (*D*), melittin at $P/L = 1:7$ (*E*), lysozyme at $P/L = 1:7$ (*F*), and cytochrome *c* at $P/L = 1:7$ (*G*). Lipid composition of the SLBs was SOPC/POPG/NBD-PC, 78:20:2 (mol/mol). The inset in *E* is a twofold magnification relative to the main image. The inset in *F* shows the intensity profile along the horizontal black line.

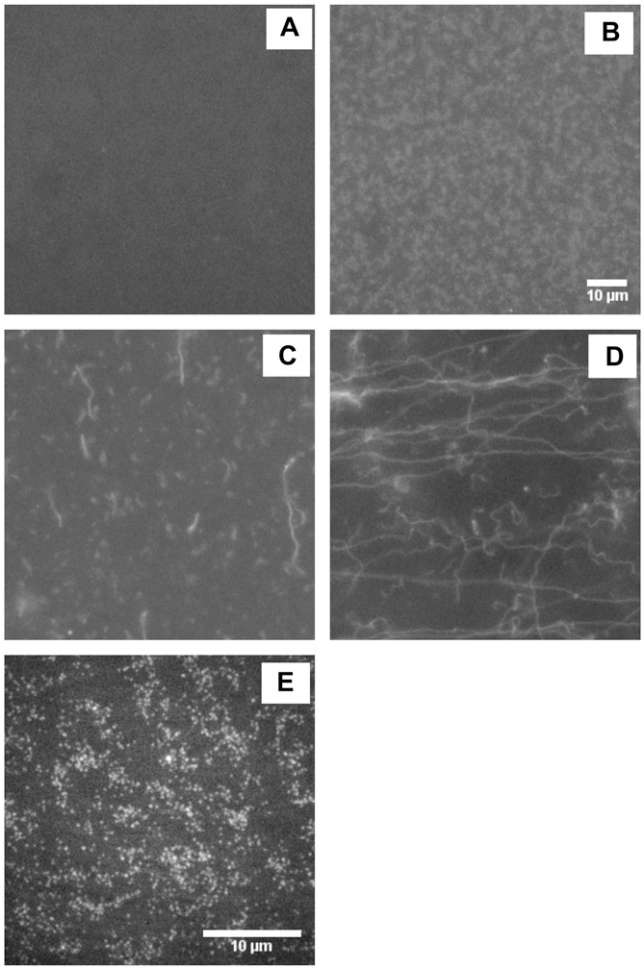


FIGURE 5 Progressive elongation of lipid nanotubules as a function of peptide concentration in the bathing solution. The fluorescence images were taken before peptide addition (*A*) and after adding C-temB-K temporin B variant at $P/L = 1{:}4.7$ (*B* and *E*), 1:2.8 (*C*), and 1:1.4 (*D*). Lipid composition of the bilayer was SOPC/POPG/NBD-PC, 78:20:2 (mol/mol). Note that images were acquired at different regions of the bilayer. Differences in the intensity of the surface fluorescence (background in *B–D*) are mainly the result of rapid photobleaching of NBD. Filaments in *D* are seen to be partially aligned with the direction of liquid flow during peptide addition and mixing. Panel *E* shows high-resolution confocal image of NBD fluorescence in a sample similar to the one in panel *B*.

more homogeneous. Finally, after the addition of a total of 1.7 $\mu$M of peptide ($P/L = 1{:}1.4$), numerous long tubules were observed. The concentration dependence was strongly influenced by the peptide sequence. Accordingly, whereas ~1.7 $\mu$M of C-temB-K was used above, only ~0.3 $\mu$M ($P/L = 1{:}7.8$) of wt temporin B was needed to obtain a similar effect (Fig. 2).

Data obtained for different peptides from a series of observations on SLBs are summarized in Table 1.

### Localization of adsorbed peptides

To determine the distribution of the peptides in the lipid membrane and during the subsequent morphological transformations, a temporin B variant labeled with the Texas red fluorophore was used. The absorbance and emission of Texas red are well separated from those of NBD, thus allowing two-color imaging of these fluorophores, with fluorescence images of the same SLB area observed in the green or red channel (Fig. 6). As illustrated above, when the peptide concentration is below a certain threshold, no lipid tubules form, and microscopic domains of higher fluorescence intensity appear in the bilayer, most likely representing areas with increased local surface density of lipids (Fig. 6 *A*). Interestingly, the same area imaged in the red channel for the localization of the fluorescent peptide (Fig. 6 *B*) exhibits spots of decreased fluorescence exactly coinciding with the bright spots in the green channel. Accordingly, the areas enriched in lipids appear to be depleted of peptide, and vice versa, as demonstrated by superimposing the images from red and green channels (Fig. 6 *C*). This observation could further be confirmed using digital colocalization analysis after inversion of one of the input images (25). After further addition of the peptide, tubular protrusions become visible in both channels (Fig. 6, *D* and *E*), revealing these structures to be composed of both lipids and peptides. At this stage the background fluorescence from the surface becomes more homogeneous, indicating that the segregation of the peptide and lipid in the plane of the bilayer is partially relieved.

### Effect of lipid composition

Acidic phospholipids have been demonstrated to promote the membrane association of the peptides used in the above experiments. Accordingly, it was of interest to investigate the effect of the lipid composition of SLBs on the tubule formation described above. Interestingly, for SLBs composed of zwitterionic PC (Fig. 7 *A*) temB causes the formation of large ($>1$ $\mu$m) vesicular structures as well as a somewhat reduced number of tubules. Yet compared to PC/PG bilayers, longer exposure to peptide and/or higher flow rate is needed for neat PC SLBs. In keeping with its truncated cone-like effective molecular shape, cardiolipin (CL), another abundant acidic phospholipid of bacterial membranes, is known to have a negative spontaneous curvature, which is manifested, in particular, in its propensity to form an inverted hexagonal phase in the presence of divalent cations (26). Substitution of PG by CL also changes the nature of membrane perturbation by temB (Fig. 7 *B*). More specifically, for PC/CL (8:2, mol/mol) SLB, only very few tubules are observed, yet the fluorescence decrease on exposure of the SLB to temB is significant. Another phospholipid with negative spontaneous curvature is phosphatidylethanolamine (PE). Presence of the latter lipid in SLBs inhibited tubule formation (Fig. 7 *C*), and instead a large number of smaller structures (seemingly small vesicles) were formed.

## DISCUSSION

Amphiphilic molecules, and lipids in particular, are known to self-organize in aqueous environments, adopting a variety

**TABLE 1 Approximate threshold amounts (*P/L*) of membrane-active peptides and proteins needed to induce the indicated morphological changes for glass-supported PC/PG (8:2) bilayers**

| Peptide/protein | Uneven surface density of lipid | Thin tubules | Thick tubules/cylinders | Multilamellar vesicles | Multilayer stacks |
|---|---|---|---|---|---|
| wt-temB | <1:7.8* | 1:7.8 | <1:2.3 | No | No |
| C-temB-COOH | 1:2.8 | >1:1 (rare) | >1:1 (rare) | 1:1 | No |
| C-temB-K | <1:4.7 | 1:2.8 | 1:2.8 | 1:1.4 (rare) | No |
| temL | <1:7 | 1:7 (rare) | 1:2.8 | 1:2.8 | No |
| Melittin | No | 1:7 | >1:7 | >1:7 | No |
| Lysozyme | No | No | No | No | <1:7 |
| Cytochrome *c* | No | No | No | No | >1:7 |

*Expressed as molar ratios of total (nominal) peptide to total lipid.

of structures of different geometries and properties (27). Changes in physicochemical parameters (e.g., temperature, chemical structure of amphiphilic molecules, and ion composition of aqueous phase) may further induce interconversions between the various types of organization. Of these self-assembled structures, tubules formed by amphiphilic molecules have only recently attracted more attention yet demonstrate great potential in nanofabrication techniques in electronic engineering, drug delivery, and analytical applications (28,29). Here we demonstrate, using fluorescence microscopy, the transformation of solid-supported phospholipid bilayers by antimicrobial peptides to long fibrillar structures, incorporating both lipids and peptide. These fibrillar structures could represent long cylindrical micelles made by a single cylindrical leaflet of lipids, with the lipid alkyl chains forming the hydrophobic interior of the micelle (27). Yet, our observations of the high plasticity of the tubules, including their remarkable stretchability as well as micropipette-induced deformations (see Movie 3 in Supplementary Material) provide support for a tubular geometry, where a closed lipid bilayer forms a tube with the lipid leaflets surrounding an aqueous core. Because the diameter of the tubules is below the resolution limit of our optical setup, i.e., below ~250 nm, we refer to these structures as nanotubules.

The mechanical basis for higher plasticity of tubules as opposed to cylindrical micelles can be rationalized as follows. To have a lipid-water system in equilibrium during membrane shape transformations, the volume of the hydrocarbon chains and the surface area per lipid should remain constant at their equilibrium values. If the area per lipid increases above the equilibrium value, the hydrocarbon chains become exposed to aqueous environment, resulting in a drastic decrease of entropy (27). On stretching a cylindrical micelle, in order to keep the hydrocarbon volume constant, the area of lipid-water interface has to increase proportionally to the square root of length, which is associated with a high energy cost of monolayer stretching deformation. On the other hand, when bilayer tubule is stretched, it can maintain both total interfacial area and hydrocarbon volume constant at the expense of its diameter decreasing proportionally to the increase in length. The energy cost associated with the latter process is mainly the energy of the bilayer bending deformation. In brief, the free energy of elastic stretching of a cylindrical micelle, e.g., from $l_0 = 1\ \mu$m to $l_1 = 2\ \mu$m, can be approximated by $E_{\text{micelle}} = \pi l_{\text{hc}} l_0 k_{\text{a}} (\sqrt{2} - 1)^2/\sqrt{2}$, where $l_{\text{hc}}$ is the radius of the hydrocarbon core of the micelle, and $k_{\text{a}}$ is the membrane surface tension (per monolayer). Corresponding energy of bending deformation caused by the stretching of a bilayer tubule is $E_{\text{tubule}} = \pi r_0 l_0 k_{\text{b}} (1/r_1 - 1/r_0)^2$, where $k_{\text{b}}$ is the bending rigidity of a bilayer, and $r_0$ and $r_1$ are the tubule radii before and after stretching ($r_1 = r_0/2$ when the tubule length increases twofold). By taking measured values for $k_{\text{a}} = 0.1\ \text{J/m}^2$, $k_{\text{b}} = 5\times10^{-20}$ J (27), $r_0 = 50$ nm, and $l_{\text{hc}} = 1.5$ nm, the ratio of the corresponding stretching energies is found to be $E_{\text{micelle}}/E_{\text{tubule}} = 18$. Thus, for the geometries of the structures relevant to the current study, these processes appear to differ by more than an order of magnitude in free energy cost.

The freely floating lipid-peptide tubules are able to maintain their prolate shape because the peptides inserted in their outer monolayer induce positive curvature strain, i.e., change its spontaneous curvature to significantly positive values, which means that such strained membranes would achieve equilibrium only by adopting a highly curved shape. The simplest high-curvature geometry for a continuous bilayer is a tube. Additional argument in favor of the tubular geometry may be obtained from the comparison of the persistence length of the observed structures with the literature data on the persistence lengths of lipid tubules and cylindrical (worm-like) micelles. The persistence length of the temporin B–induced protrusions is on the order of 1–5 $\mu$m, as mentioned in the Results section. The persistence length of a lipid bilayer tube can be calculated as $\pi r k_{\text{b}}/kT$, where $r$ is the tube radius (30). Taking $k_{\text{b}} = 10kT$ (27) and $r$ in the range of 10–100 nm, we get persistence length of 0.3–3 $\mu$m, in excellent agreement with our estimate from experimental data. In contrast, relevant cylindrical micellar structures have persistence lengths on the order of tens of nanometers (31,32).

What provides the driving force for the observed morphological changes induced by the antimicrobial peptides? Both temporin B and temporin L are short cationic peptides having no secondary structure in aqueous solutions. However, on binding to lipids or in water-trifluoroethanol mixtures, they form amphipathic $\alpha$-helices and are known to intercalate into

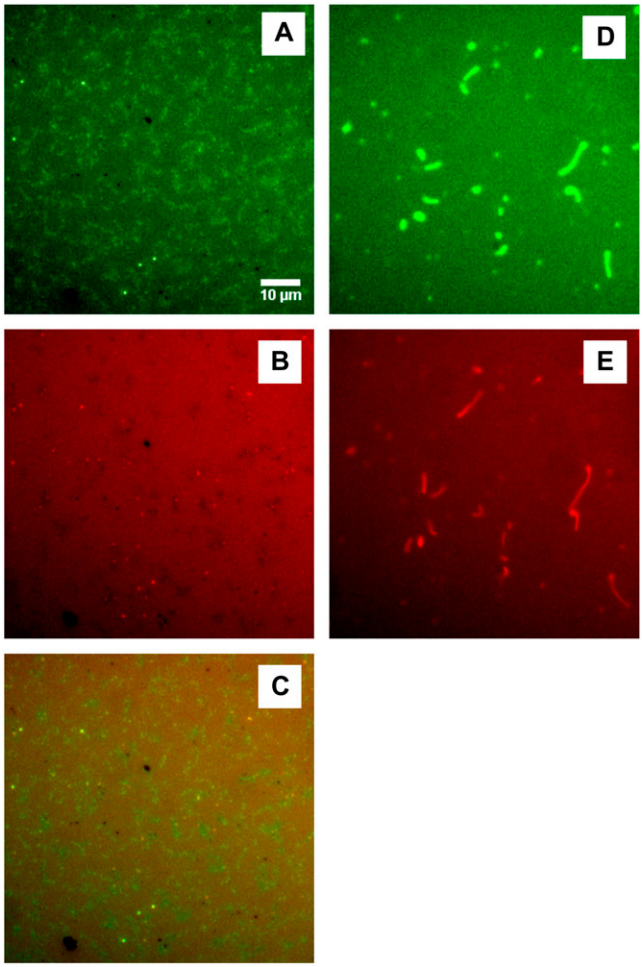


FIGURE 6 Pseudocolor visualization of fluorescent temporin B and lipid derivatives in SLBs. NBD-labeled lipids were visualized using the green channel (*A* and *D*), and the red channel was used to observe Texas red-labeled temporin B (*B* and *E*). Imaging was performed at the stage of lipid segregation (*A* and *B*) and at the stage of tubule formation (*D* and *E*). The images were pseudocolored using image-processing software. Panel *C* represents pixel-by-pixel superposition of images in panels *A* and *B*. Lipid composition of the bilayer was SOPC/POPG/NBD-PC, 78:20:2 (mol/mol). Occasional black spots and very bright dots are bilayer defects present before the peptide addition.

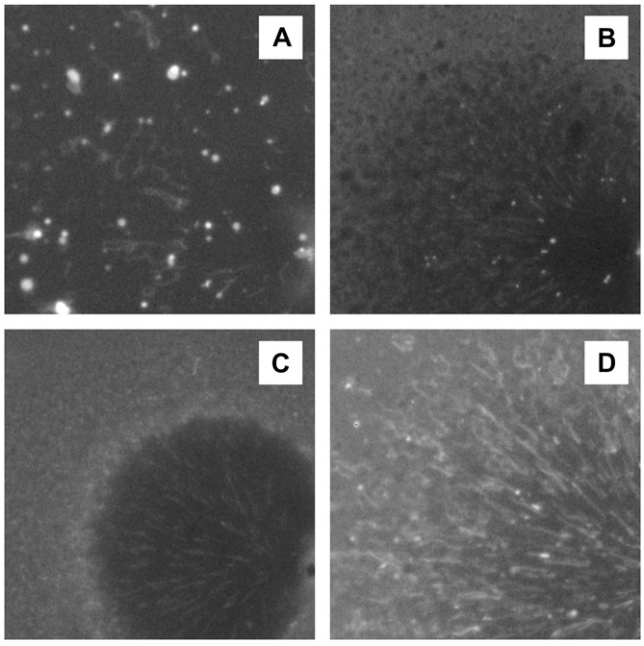


FIGURE 7 Topical application of temporin B onto supported bilayers with different phospholipid compositions. Temporin B solution (20 $\mu$M) was applied continuously with a flow rate of ~100 nl/s. Micropipette tip is located in the lower right corner of the images. Images were acquired at the indicated times after the beginning of peptide application over the SLBs composed of SOPC/NBD-PC, 98:2 (after 10 s, *A*), SOPC/CL/NBD-PC, 78:20:2 (after 2 s, *B*), SOPC/POPE/POPG/NBD-PC, 28:50:20:2 (after 2 s, *C*), and SOPC/POPG/NBD-PG, 80:18:2 (after 2 s, *D*).

lipid membranes (13,33). In a membrane environment and at low P/L ratios, these peptides orient with their helix axis parallel to the membrane surface (34). Detailed studies on the interactions of the above antimicrobial peptides with lipid monolayers at the air-water interface have been performed previously in our laboratory (10). Monolayer experiments show that these peptides cause a significant increase in surface pressure under constant-area conditions, with the magnitude of this increment diminishing when the initial pressure of the monolayer increases. For temB and an SOPC/POPG (8:2) film, the monolayer exclusion pressure, i.e., the limiting initial lateral packing of lipid at which the peptide no longer inserts into the lipid monolayer (35), was estimated at 54 mN/m (10). This value is significantly higher than the estimate for the equilibrium surface pressure in bilayer vesicles, ~35 mN/m (36), and therefore a considerable insertion of temporins B and L into the SLBs is expected. Accordingly, this should cause a substantial increase in the lateral packing in the resulting lipid-peptide composite membrane. In addition, localization of the amphiphilic peptides within the polar/apolar interface of the outer phospholipid leaflet of the SLB would cause a change in the lateral pressure profile across the monolayer, increasing the pressure in the interfacial region and lowering it in the hydrophobic core. This strain caused by increased net lateral pressure and altered pressure profile across the membrane can be relieved in two ways: by the monolayer dilation and concomitant membrane thinning (37), providing that such dilation is not restricted, and/or by protrusion of the membrane out of the support and adoption of a structure with an overall positive curvature (38–40). Our microscopy observations provide support in favor of both of the above processes, the latter being observed at higher P/L ratios.

Membrane thinning caused by antimicrobial peptides was first observed by Huang et al. for magainin 2 and alamethicin (41,42), and subsequent studies have revealed this ability for various amphiphilic peptides including $\alpha$-helical peptides in the so-called S state, residing parallel to the membrane

surface and embedded in the interfacial region (43,44). By decreasing its thickness, the bilayer accommodates the interfacial area expansion caused by the peptide insertion while keeping the volume of lipid hydrocarbon chains constant. Membrane thinning has been shown to be roughly proportional to P/L (43). In addition, both theoretical analysis (45) and AFM measurements on supported lipid bilayers (44) have revealed that membrane thinning can mediate peptide lateral segregation into distinct domains with reduced thickness. Our fluorescence microscopy observations are consistent with the membrane-thinning effect of temporin B and its derivatives on SLBs. Indeed, upon two-color imaging at low amounts of peptide, we observed a clear initial segregation of red and green fluorescence (Fig. 6, *A–C*), corresponding to domains enriched in the peptide and fluorescent lipid (devoid of peptide), respectively. This situation is schematically depicted in Fig. 8 *A*, where the peptide helices in an SLB are shown with their hydrophobic facets in gray. Heterogeneity of lipid fluorescence was also observed when using the unlabeled peptide (Fig. 5 *B*). In a similar manner, following a topical application of the antimicrobial peptides on an SLB, the expanding circles of decreased fluorescence should correspond to a diminished lipid surface density (Fig. 7) as a result of membrane thinning in the area exposed to the applied peptide.

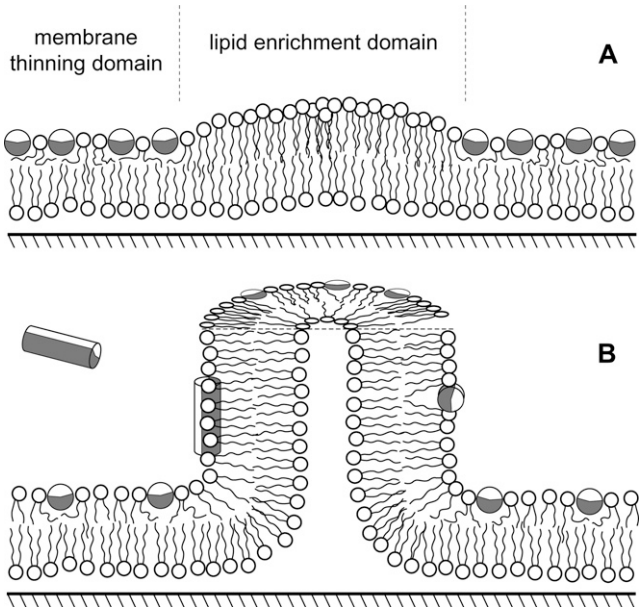


FIGURE 8 Tentative mechanism of tubule outgrowth from a supported membrane induced by amphiphilic $\alpha$-helical peptides. Peptide $\alpha$-helices are represented by cylinders with their hydrophobic sides shaded gray. (*A*) For low peptide/lipid ratios ($P/L < 1{:}5$), segregation of bound peptides into domains enriched in lipid and lipid-protein arrays together with membrane thinning take place. (*B*) At $P/L > 1{:}5$, augmented molecular packing (lateral pressure) and positive curvature strain trigger the outgrowth of tubular membrane protrusion from the planar bilayer, with the bound protein redistributing over the SLB and the tubules.

On further binding and insertion of the amphipathic peptide into the membrane, the resulting augmented molecular packing and molecular crowding can no longer be sustained by a planar geometry, causing the outgrowth and elongation of nanotubules from the SLB (Fig. 8 *B*). Notably, this transformation relieves excess surface pressure as well as the positive curvature strain in the upper leaflet of the supported bilayer. Although only the outer leaflet of the bilayer may be initially influenced by the peptide insertion, both leaflets undergo shape transformation because of the coupling of the leaflets in the bilayer (46). Because of the difference in the lateral pressure between the two leaflets, we may also expect augmented transfer of lipid from the outer to the inner monolayer (the latter contacting the solid support) via the defects in SLB, which are likely to be numerous as suggested by the electrochemical, AFM, and fluorescence (NBD reduction with dithionite) studies (19,47). Another possible pathway for the relief of excess surface pressure is the dilation of the outer monolayer or the bilayer as a whole. However, during the binding of the peptide to SLB, complete dilation is likely to be retarded by the viscous friction between the upper and lower monolayers (48) and by the pinning of the bilayer to the support (49).

Another intriguing characteristic of the above tubules is that we never observed them to branch. The mechanistic basis for this feature of the tubules is uncertain yet could relate to the tendency of these peptides to arrange into linear arrays. More specifically, we have recently reported several antimicrobial peptides to form amyloid-type fibrils in the presence of liposomes containing acidic phospholipids (50,51). These amyloid-like fibers have diameters on the micrometer scale and incorporate lipid from the liposomes (50,52). Our further studies in this area revealed this property also for temB (R. Sood, Y.A. Domanov, and P. K. J. Kinnunen, unpublished data). The linear, nonbranching organization of lipids and peptides in the observed lipid-peptide nanotubules further suggests that they may represent an intermediate stage in the formation of the amyloid-like fibers by these peptides.

In accordance with the available literature for different model lipid membranes (see below), our current results with SLBs demonstrate that lipid-peptide interactions alone can provide a driving force for spontaneous membrane shape transformations in the absence of any external pulling force. Moreover, the transformation can be effectively regulated by the lipid composition of the membrane and the peptide structure. In particular, our observations demonstrate that spontaneous curvature of peptide-free bilayer can affect the morphology of membrane perturbations. As shown for SLBs composed of SOPC/POPG, 8:2 mol/mol, temporin B induces numerous stable tubular structures (Fig. 3, *A–D*, Fig. 7 *D*). On the other hand, for an SLB that contains cardiolipin, a lipid with negative spontaneous curvature, the formation of stable tubular structures was not observed (Fig. 7 *B*). In a similar manner, the presence of PE in the SLB efficiently inhibits tubule growth (Fig. 7 *C*). Still, some occasional tubules are seen in

SLBs with CL or PE, but in contrast to PC/PG and neat PC bilayers, these tubules are very scanty and unstable, maintaining a tubular geometry for no more than a few seconds after the addition of the antimicrobial peptide. This lack of tubule formation could be explained by the insertion of the AMP into a bilayer containing cone-shaped lipids failing to develop a sufficient positive curvature strain, necessary for the formation of strongly curved structures in the outer leaflet of the tubules. Because for both CL and PE the membrane thinning and release of lipid particles occur, it appears that the overall dilation of the membrane does take place, yet the negative curvature strain imposed by these lipids prevents the formation of the tubular structures. Interestingly, disruption of membranes by positive curvature strain induced by antimicrobial peptides has been recently observed by $^{31}$P-NMR and DSC (53–56), where amphipathic $\alpha$-helical peptides MSI-78, MSI-843, and MSI-594 hindered the fluid lamellar to inverted hexagonal ($L_\alpha \rightarrow H_{II}$) phase transition for PE while promoting the formation of the normal hexagonal phase ($H_I$) in PC. Furthermore, it appears that different peptides can destabilize bilayer membranes by two opposing mechanisms, depending on the peptide structure: whereas peptides like temporin B, MSI-78, MSI-594, MSI-843, and LL-37 (57) induce positive curvature strain (MSI-78 is also known to cause membrane thinning), another class of peptides including paradaxin (58), tachyplesin (59), and polyphemusins (60) induce negative curvature strain in the bilayer. In this context it is of interest to compare our findings to those made for MSI-78 (53), as the latter peptide and temporin B have very similar physicochemical properties (strong amphipathicity, positive charge). MSI-78 has been demonstrated to promote the formation of $H_I$ phase, i.e., cylindrical micelles with a hydrophobic interior. Although the driving forces in both cases are likely to be the same, the $H_I$ phase is topologically distinct from the bilayer tubules. However, because of the different methods of sample preparation, direct comparison is ambiguous. More specifically, our experiments were performed on single supported bilayers in excess water, whereas Hallock et al. used weakly hydrated stacks of bilayers (with a few tens of water molecules per lipid) sandwiched between two glass surfaces. In fact, FTIR studies have demonstrated that the mode of lipid-peptide interactions differs substantially between the weakly hydrated multibilayers and the single bilayers in the excess water (61).

In addition to lipid specificity of the tubulation, we observed a strong variation of the membrane response to different peptides and proteins tested in this study. The lack of membrane transformation by C-temB-COOH (with carboxyl substituted for C-terminal amide) reveals the significance of sufficient positive charge of the peptide for the membrane perturbation. Tubular structures similar to those caused by temB were also induced by melittin. Because melittin bears no relation to the temporin family, this suggests that tubule formation may represent a rather general property of a range of amphiphilic cationic peptides (38). However, water-soluble polycationic proteins cytochrome *c* and lysozyme give rise to a different mode of bilayer perturbation, our observations suggesting that they induce the squeezing out of the SLB of flat multibilayer structures stacked on the parent bilayer. Similar structures have been observed on contraction of lipid monolayers containing surfactant proteins B and C (62,63).

The biological significance of our findings remains uncertain at this stage, yet the outgrowth of tubules could be involved in the mechanisms of perturbation of bacterial membranes by these peptides. In this regard the lipid selectivity of this process is of interest, and we are currently exploring this issue in more detail. Prevention of tubule formation by 50% POPE in the supported bilayers may be related to the selectivity of temporin B against bacteria, relevant with respect to the difference in PE content of the membranes of gram-positive and gram-negative bacteria. However, extensive additional experiments with various lipid compositions, as well as comparison of different membranes (e.g., vesicles and bacteria), are mandatory to establish any causalities. These types of mechanisms could also be involved in membrane transformations in eukaryotic cells. It is known that cells are able to develop and maintain dynamic networks involving tubular structures both extending out of their plasma membrane and intracellularly connecting different organelles, involved along with vesicular carriers in a number of important intracellular trafficking routes (64). An interesting example of intercellular communication by means of dynamically forming lipid nanotubules has recently been reported (65). Futhermore, dynamically forming lipid nanotubules have been shown to represent a major means of communication between the stacks of cisternae in Golgi apparatus as well as in the retrograde traffic of membranes from Golgi to endoplasmic reticulum, visualized using GFP fusion proteins (66). Combined light and electron microscopy revealed tubular interconnections dynamically forming between cisternae in a stack during an induced traffic wave (67), and these tubular continuities were suggested to play a key role in the recycling of Golgi enzymes (68). Obviously, several mechanisms are likely to account for the formation and maintenance of the above dynamic structures, involving the inherent properties of both lipids and proteins. Using optical microscopy, Akiyoshi et al. observed spontaneous formation of tubular lipid structures connecting liposomes and forming complex networks in the presence of gangliosides (69) or cholesterol (70) mixed with PC. Orwar et al. have elaborated a set of tools and procedures allowing forced retraction of lipid nanotubules from giant liposomes and subsequent manipulation of the liposome-tubule networks (28,71). There is also evidence that in vivo the opposing activities of cytoplasmic phospholipase $A_2$ and lysophospholipid acyltransferase can regulate membrane shape transformations by changing the lysophospholipid content of membranes, thus affecting their spontaneous curvature (64,72). Interestingly, transformation of liposomes composed of egg yolk PC, mixtures of PC and PG, and mixtures of

Golgi-specific phospholipids into long nanotubular structures after interaction with the amphiphilic $\alpha$-helical peptide Hel 13-5 has been demonstrated (38,39,73). These authors have suggested that this membrane transformation could be related to the morphogenesis of the tubular structures of Golgi apparatus in cells.

Roux and co-workers were able to construct an in vitro minimal system allowing membrane tubulation with molecular motor kinesin pulling on giant liposomes (74,75). Although this is likely to represent a major means of directing the tubule growth in the cell, other mechanisms of initial tubule formation are possible. In accordance with recent results mentioned above (38–40,69,70,73) and studies reviewed by Brown et al. (64), our observations demonstrate that the initial tubule formation is possible in the absence of any pulling machinery. Likewise, tubular budding of erythrocyte membrane induced by nonionic surfactant dodecylmaltoside was observed using TEM (40) and is most likely driven by the membrane expansion and positive curvature strain imposed by the surfactant insertion in the outer leaflet of the erythrocyte membrane. It is tempting to speculate that peptide-induced membrane shape transformations could also be involved in processes such as neurite outgrowth. More specifically, although the dynamic polymerization and depolymerization of F-actin and tubulin provide a structural support for newly forming neurites (76), they may not be sufficient for the initiation of the neural membrane transformation or for the elongation of the tubular processes. In other words, the cytoskeletal elements could be secondary to initial membrane transformations rather than being the primary factor pushing the membrane from the inside and providing a driving force for the elongation. Membrane-active peptide gradients in the neural tissue could be involved in directing neurite outgrowth and thus chemically pattern the development on new interneuron connections, in parallel with specific ligand-receptor guiding systems (77). In fact, Liesi et al. (78) have demonstrated that a synthetic amphiphilic peptide derived from laminin, an extracellular matrix protein, stimulates the outgrowth of neurites in mouse neuron cultures at concentrations comparable to those used in our study.

## CONCLUSIONS

This study represents the first report on the formation of bilayer lipid nanotubules from solid-supported bilayer membranes triggered by the membrane interaction with amphiphilic cationic peptides. The well-defined geometry of our experimental system allows us to conclude that amphiphilic peptide-lipid interactions alone can provide a driving force for the spontaneous membrane shape transformations leading to tubule outgrowth and elongation, requiring no external pulling or pushing force. Experiments with different membrane lipid compositions provide evidence for the primary role of positive curvature strain in the tubulation process. In addition to the membrane perturbation of bacteria by antimicrobial peptides, this process, driven by proper amphiphilic peptides, could also play an important role in morphogenesis and stability of intracellular tubular structures as well as in the intercellular communication.

The authors are grateful to Dr. Ove Eriksson for his help with mass spectrometry analysis of the peptides.

The Helsinki Biophysics & Biomembrane Group is supported by the Finnish Academy and the Sigrid Jusélius Foundation.

## REFERENCES

1. Yeaman, M. R., and N. Y. Yount. 2003. Mechanisms of antimicrobial peptide action and resistance. *Pharmacol. Rev.* 55:27–55.
2. Brown, K. L., and R. E. Hancock. 2006. Cationic host defense (antimicrobial) peptides. *Curr. Opin. Immunol.* 18:24–30.
3. van't Hof, W., E. C. Veerman, E. J. Helmerhorst, and A. V. Amerongen. 2001. Antimicrobial peptides: Properties and applicability. *Biol. Chem.* 382:597–619.
4. Shai, Y. 1999. Mechanism of the binding, insertion and destabilization of phospholipid bilayer membranes by alpha-helical antimicrobial and cell non-selective membrane-lytic peptides. *Biochim. Biophys. Acta.* 1462:55–70.
5. Epand, R. M., and H. J. Vogel. 1999. Diversity of antimicrobial peptides and their mechanisms of action. *Biochim. Biophys. Acta.* 1462: 11–28.
6. Dathe, M., and T. Wieprecht. 1999. Structural features of helical antimicrobial peptides: Their potential to modulate activity on model membranes and biological cells. *Biochim. Biophys. Acta.* 1462: 71–87.
7. Sitaram, N., and R. Nagaraj. 1999. Interaction of antimicrobial peptides with biological and model membranes: Structural and charge requirements for activity. *Biochim. Biophys. Acta.* 1462:29–54.
8. Simmaco, M., G. Mignogna, S. Canofeni, R. Miele, M. L. Mangoni, and D. Barra. 1996. Temporins, antimicrobial peptides from the European red frog *Rana temporaria*. *Eur. J. Biochem.* 242:788–792.
9. Rinaldi, A. C., A. Di Giulio, M. Liberi, G. Gualtieri, A. Oratore, A. Bozzi, M. E. Schininà, and M. Simmaco. 2001. Effects of temporins on molecular dynamics and membrane permeabilization in lipid vesicles. *J. Pept. Res.* 58:213–220.
10. Zhao, H., A. C. Rinaldi, A. Di Giulio, M. Simmaco, and P. K. J. Kinnunen. 2002. Interactions of the antimicrobial peptides temporins with model biomembranes. Comparison of temporins B and L. *Biochemistry.* 41:4425–4436.
11. Rinaldi, A. C., M. L. Mangoni, A. Rufo, C. Luzi, D. Barra, H. Zhao, P. K. J. Kinnunen, A. Bozzi, A. Di Giulio, and M. Simmaco. 2002. Temporin L: Antimicrobial, haemolytic and cytotoxic activities, and effects on membrane permeabilization in lipid vesicles. *Biochem. J.* 368:91–100.
12. Mangoni, M. L., J. M. Saugar, M. Dellisanti, D. Barra, M. Simmaco, and L. Rivas. 2005. Temporins, small antimicrobial peptides with leishmanicidal activity. *J. Biol. Chem.* 280:984–990.
13. Mangoni, M. L., A. C. Rinaldi, A. Di Giulio, G. Mignogna, A. Bozzi, D. Barra, and M. Simmaco. 2000. Structure-function relationships of temporins, small antimicrobial peptides from amphibian skin. *Eur. J. Biochem.* 267:1447–1454.
14. Zhao, H., and P. K. J. Kinnunen. 2003. Modulation of the activity of secretory phospholipase $A_2$ by antimicrobial peptides. *Antimicrob. Agents Chemother.* 47:965–971.
15. Epand, R. M., and R. F. Epand. 2003. Liposomes as models for antimicrobial peptides. *Methods Enzymol.* 372:124–133.
16. Zhao, H., J. Mattila, J. M. Holopainen, and P. K. J. Kinnunen. 2001. Comparison of the membrane association of two antimicrobial peptides, magainin 2 and indolicidin. *Biophys. J.* 81:2979–2991.

17. Brian, A. A., and H. M. McConnell. 1984. Allogeneic stimulation of cytotoxic T cells by supported planar membranes. *Proc. Natl. Acad. Sci. USA*. 81:6159–6163.

18. Richter, R., A. Mukhopadhyay, and A. Brisson. 2003. Pathways of lipid vesicle deposition on solid surfaces: A combined QCM-D and AFM study. *Biophys. J.* 85:3035–3047.

19. Nollert, P., H. Kiefer, and F. Jähnig. 1995. Lipid vesicle adsorption versus formation of planar bilayers on solid surfaces. *Biophys. J.* 69: 1447–1455.

20. Nagle, J. F., and S. Tristram-Nagle. 2000. Structure of lipid bilayers. *Biochim. Biophys. Acta*. 1469:159–195.

21. ImageJ. Public domain java image processing program. 2005. http://rsb.info.nih.gov/ij. [Online].

22. Vogel, H., and F. Jähnig. 1986. The structure of melittin in membranes. *Biophys. J.* 50:573–582.

23. Matsuzaki, K., S. Yoneyama, and K. Miyajima. 1997. Pore formation and translocation of melittin. *Biophys. J.* 73:831–838.

24. Hristova, K., C. E. Dempsey, and S. H. White. 2001. Structure, location, and lipid perturbations of melittin at the membrane interface. *Biophys. J.* 80:801–811.

25. Colocalization plugin for ImageJ. 2004. http://rsb.info.nih.gov/ij/plugins/colocalization.html. [Online].

26. Ortiz, A., J. A. Killian, A. J. Verkleij, and J. Wilschut. 1999. Membrane fusion and the lamellar-to-inverted-hexagonal phase transition in cardiolipin vesicle systems induced by divalent cations. *Biophys. J.* 77:2003–2014.

27. Israelachvili, J. N. 1992. Intermolecular and Surface Forces. Academic Press, London, UK.

28. Karlsson, M., M. Davidson, R. Karlsson, A. Karlsson, J. Bergenholtz, Z. Konkoli, A. Jesorka, T. Lobovkina, J. Hurtig, M. Voinova, and O. Orwar. 2004. Biomimetic nanoscale reactors and networks. *Annu. Rev. Phys. Chem.* 55:613–649.

29. Shimizu, T., M. Masuda, and H. Minamikawa. 2005. Supramolecular nanotube architectures based on amphiphilic molecules. *Chem. Rev.* 105: 1401–1443.

30. Derényi, I., F. Jülicher, and J. Prost. 2002. Formation and interaction of membrane tubes. *Phys. Rev. Lett.* 88:238101.

31. Cohen, D. E., G. M. Thurston, R. A. Chamberlin, G. B. Benedek, and M. C. Carey. 1998. Laser light scattering evidence for a common wormlike growth structure of mixed micelles in bile salt- and straight-chain detergent-phosphatidylcholine aqueous systems: Relevance to the micellar structure of bile. *Biochemistry*. 37:14798–14814.

32. Boek, E. S., W. K. den Otter, W. J. Briels, and D. Iakovlev. 2004. Molecular-dynamics simulation of amphiphilic bilayer membranes and wormlike micelles: a multi-scale modelling approach to the design of viscoelastic surfactant solutions. *Phil. Trans. R. Soc. A*. 362:1625–1638.

33. Zhao, H., and P. K. J. Kinnunen. 2002. Binding of the antimicrobial peptide temporin L to liposomes assessed by Trp fluorescence. *J. Biol. Chem.* 277:25170–25177.

34. Castano, S., B. Desbat, M. Laguerre, and J. Dufourcq. 1999. Structure, orientation and affinity for interfaces and lipids of ideally amphipathic lytic $L_iK_j(i = 2j)$ peptides. *Biochim. Biophys. Acta*. 1416:176–194.

35. Brockman, H. 1999. Lipid monolayers: why use half a membrane to characterize protein-membrane interactions? *Curr. Opin. Struct. Biol.* 9:438–443.

36. Marsh, D. 1996. Lateral pressure in membranes. *Biochim. Biophys. Acta*. 1286:183–223.

37. Lee, M. T., W. C. Hung, F. Y. Chen, and H. W. Huang. 2005. Many-body effect of antimicrobial peptides: On the correlation between lipid's spontaneous curvature and pore formation. *Biophys. J.* 89:4006–4016.

38. Furuya, T., T. Kiyota, S. Lee, T. Inoue, G. Sugihara, A. Logvinova, P. Goldsmith, and H. M. Ellerby. 2003. Nanotubules formed by highly hydrophobic amphiphilic alpha-helical peptides and natural phospholipids. *Biophys. J.* 84:1950–1959.

39. Lee, S., T. Furuya, T. Kiyota, N. Takami, K. Murata, Y. Niidome, D. E. Bredesen, H. M. Ellerby, and G. Sugihara. 2001. De novo-designed peptide transforms Golgi-specific lipids into Golgi-like nanotubules. *J. Biol. Chem.* 276:41224–41228.

40. Kralj-Iglič, V., H. Hägerstrand, P. Veranič, K. Jezernik, B. Babnik, D. R. Gauger, and A. Iglič. 2005. Amphiphile-induced tubular budding of the bilayer membrane. *Eur. Biophys. J.* 34:1066–1070.

41. Ludtke, S., K. He, and H. Huang. 1995. Membrane thinning caused by magainin 2. *Biochemistry*. 34:16764–16769.

42. He, K., S. J. Ludtke, W. T. Heller, and H. W. Huang. 1996. Mechanism of alamethicin insertion into lipid bilayers. *Biophys. J.* 71:2669–2679.

43. Chen, F. Y., M. T. Lee, and H. W. Huang. 2003. Evidence for membrane thinning effect as the mechanism for peptide-induced pore formation. *Biophys. J.* 84:3751–3758.

44. Mecke, A., D.-K. Lee, A. Ramamoorthy, B. G. Orr, and M. M. Banaszak Holl. 2005. Membrane thinning due to antimicrobial peptide binding: An atomic force microscopy study of MSI-78 in lipid bilayers. *Biophys. J.* 89:4043–4050.

45. Zemel, A., A. Ben-Shaul, and S. May. 2004. Membrane perturbation induced by interfacially adsorbed peptides. *Biophys. J.* 86:3607–3619.

46. Sheetz, M. P., and S. J. Singer. 1974. Biological membranes as bilayer couples. A molecular mechanism of drug-erythrocyte interactions. *Proc. Natl. Acad. Sci. USA*. 71:4457–4461.

47. Reviakine, I., and A. Brisson. 2000. Formation of supported phospholipid bilayers from unilamellar vesicles investigated by atomic force microscopy. *Langmuir*. 16:1806–1815.

48. Evans, E., and A. Yeung. 1994. Hidden dynamics in rapid changes of bilayer shape. *Chem. Phys. Lipids*. 73:39–56.

49. Sackmann, E. 1996. Supported membranes: Scientific and practical applications. *Science*. 271:43–48.

50. Zhao, H., E. K. Tuominen, and P. K. J. Kinnunen. 2004. Formation of amyloid fibers triggered by phosphatidylserine-containing membranes. *Biochemistry*. 43:10302–10307.

51. Zhao, H., A. Jutila, T. Nurminen, S. A. Wickström, J. Keski-Oja, and P. K. J. Kinnunen. 2005. Binding of endostatin to phosphatidylserine-containing membranes and formation of amyloid-like fibers. *Biochemistry*. 44:2857–2863.

52. Sparr, E., M. F. Engel, D. V. Sakharov, M. Sprong, J. Jacobs, B. de Kruijff, J. W. Höppener, and J. A. Killian. 2004. Islet amyloid polypeptide-induced membrane leakage involves uptake of lipids by forming amyloid fibers. *FEBS Lett.* 577:117–120.

53. Hallock, K. J., D.-K. Lee, and A. Ramamoorthy. 2003. MSI-78, an analogue of the magainin antimicrobial peptides, disrupts lipid bilayer structure via positive curvature strain. *Biophys. J.* 84:3052–3060.

54. Thennarasu, S., D. Lee, A. Tan, U. Prasad Kari, and A. Ramamoorthy. 2005. Antimicrobial activity and membrane selective interactions of a synthetic lipopeptide MSI-843. *Biochim. Biophys. Acta (Biomembranes)*. 1711:49–58.

55. Ramamoorthy, A., S. Thennarasu, D. Lee, A. Tan, and L. Maloy. 2006. Solid-state NMR investigation of the membrane-disrupting mechanism of antimicrobial peptides MSI-78 and MSI-594 derived from magainin 2 and melittin. *Biophys. J.* 91:206–216.

56. Porcelli, F., B. A. Buck-Koehntop, S. Thennarasu, A. Ramamoorthy, and G. Veglia. 2006. Structures of the dimeric and monomeric variants of magainin antimicrobial peptides (MSI-78 and MSI-594) in micelles and bilayers, determined by NMR spectroscopy. *Biochemistry*. 45:5793–5799.

57. Henzler Wildman, K. A., D. Lee, and A. Ramamoorthy. 2003. Mechanism of lipid bilayer disruption by the human antimicrobial peptide, LL-37. *Biochemistry*. 42:6545–6558.

58. Hallock, K. J., D. Lee, J. Omnaas, H. I. Mosberg, and A. Ramamoorthy. 2002. Membrane composition determines pardaxin's mechanism of lipid bilayer disruption. *Biophys. J.* 83:1004–1013.

59. Doherty, T., A. J. Waring, and M. Hong. 2006. Peptide-lipid interactions of the $\beta$-hairpin antimicrobial peptide tachyplesin and its linear derivatives from solid-state NMR. *Biochim. Biophys. Acta (Biomembranes)*. 1758:1285–1291.

60. Powers, J.-P. S., A. Tan, A. Ramamoorthy, and R. E. W. Hancock. 2005. Solution structure and interaction of the antimicrobial polyphemusins with lipid membranes. *Biochemistry*. 44:15504–15513.

61. Silvestro, L., and P. H. Axelsen. 1998. Infrared spectroscopy of supported lipid monolayer, bilayer, and multibilayer membranes. *Chem. Phys. Lipids*. 96:69–80.

62. Krol, S., M. Ross, M. Sieber, S. Kunneke, H. J. Galla, and A. Janshoff. 2000. Formation of three-dimensional protein-lipid aggregates in monolayer films induced by surfactant protein B. *Biophys. J*. 79:904–918.

63. von Nahmen, A., A. Post, H. J. Galla, and M. Sieber. 1997. The phase behavior of lipid monolayers containing pulmonary surfactant protein C studied by fluorescence light microscopy. *Eur. Biophys. J*. 26:359–369.

64. Brown, W. J., K. Chambers, and A. Doody. 2003. Phospholipase $A_2$ ($PLA_2$) enzymes in membrane trafficking: Mediators of membrane shape and function. *Traffic*. 4:214–221.

65. Rustom, A., R. Saffrich, I. Markovic, P. Walther, and H. Gerdes. 2004. Nanotubular highways for intercellular organelle transport. *Science*. 303:1007–1010.

66. Presley, J. F., C. Smith, K. Hirschberg, C. Miller, N. B. Cole, K. J. Zaal, and J. Lippincott-Schwartz. 1998. Golgi membrane dynamics. *Mol. Biol. Cell*. 9:1617–1626.

67. Trucco, A., R. S. Polishchuk, O. Martella, A. Di Pentima, A. Fusella, D. Di Giandomenico, E. San Pietro, G. V. Beznoussenko, E. V. Polishchuk, M. Baldassarre, R. Buccione, W. J. Geerts, A. J. Koster, et al. 2004. Secretory traffic triggers the formation of tubular continuities across Golgi sub-compartments. *Nat. Cell Biol.* 6:1071–1081.

68. Mironov, A. A., G. V. Beznoussenko, R. S. Polishchuk, and A. Trucco. 2005. Intra-Golgi transport: a way to a new paradigm? *Biochim. Biophys. Acta*. 1744:340–350.

69. Akiyoshi, K., A. Itaya, S. M. Nomura, N. Ono, and K. Yoshikawa. 2003. Induction of neuron-like tubes and liposome networks by cooperative effect of gangliosides and phospholipids. *FEBS Lett*. 534:33–38.

70. Nomura, S. M., Y. Mizutani, K. Kurita, A. Watanabe, and K. Akiyoshi. 2005. Changes in the morphology of cell-size liposomes in the presence of cholesterol: Formation of neuron-like tubes and liposome networks. *Biochim. Biophys. Acta*. 1669:164–169.

71. Karlsson, A., R. Karlsson, M. Karlsson, A. S. Cans, A. Strömberg, F. Ryttsén, and O. Orwar. 2001. Networks of nanotubes and containers. *Nature*. 409:150–152.

72. Drecktrah, D., K. Chambers, E. L. Racoosin, E. B. Cluett, A. Gucwa, B. Jackson, and W. J. Brown. 2003. Inhibition of a Golgi complex lysophospholipid acyltransferase induces membrane tubule formation and retrograde trafficking. *Mol. Biol. Cell*. 14:3459–3469.

73. Kitamura, A., T. Kiyota, M. Tomohiro, A. Umeda, S. Lee, T. Inoue, and G. Sugihara. 1999. Morphological behavior of acidic and neutral liposomes induced by basic amphiphilic alpha-helical peptides with systematically varied hydrophobic-hydrophilic balance. *Biophys. J*. 76: 1457–1468.

74. Roux, A., G. Cappello, J. Cartaud, J. Prost, B. Goud, and P. Bassereau. 2002. A minimal system allowing tubulation with molecular motors pulling on giant liposomes. *Proc. Natl. Acad. Sci. USA*. 99:5394–5399.

75. Leduc, C., O. Campàs, K. B. Zeldovich, A. Roux, P. Jolimaitre, L. Bourel-Bonnet, B. Goud, J.-F. Joanny, P. Bassereau, and J. Prost. 2004. Cooperative extraction of membrane nanotubes by molecular motors. *Proc. Natl. Acad. Sci. USA*. 101:17096–17101.

76. Purves, D., G. J. Augustine, D. Fitzpatrick, W. C. Hall, A. LaMantia, J. O. McNamara, and S. M. Williams. 2004. Neuroscience. D. Purves, G. J. Augustine, D. Fitzpatrick, W. C. Hall, A. LaMantia, J. O. McNamara, and S. M. Williams, editors. Sinauer Associates, Sunderland, MA.

77. Flanagan, J. G. 2006. Neural map specification by gradients. *Curr. Opin. Neurobiol.* 16:59–66.

78. Liesi, P., A. Närvänen, J. Soos, H. Sariola, and G. Snounou. 1989. Identification of a neurite outgrowth-promoting domain of laminin using synthetic peptides. *FEBS Lett*. 244:141–148.